# Advancements in biofuel research: Understanding the physical and chemical characteristics of green diesel

L. F. Ramírez-Verduzco*, G. Marroquín-Sánchez, and M. J. Hernández-Sánchez

*Instituto Mexicano del Petróleo,*
*Eje Central Norte Lázaro Cárdenas 152, San Bartolo Atepehuacan, 07730, Ciudad de México, México.*
*Dirección de Investigación en Transformación de Hidrocarburos, Gerencia de Investigación en Transformación de Biomasa.*
**e-mail: lframir@imp.mx*

Received 1 August 2023; accepted 13 March 2024

Green diesel is a potential biofuel that offers certain advantages over traditional fossil diesel, such as low environmental pollution and no sulfur. However, there is little information available regarding the density and viscosity of green diesel, which is crucial for the quality control of biofuels and their performance in engines. In this study, the properties of green diesel produced from palm and soybean oils hydrotreatment were investigated, and models were developed to predict the physical properties of green diesel and n-alkanes. The experimental measurements had uncertainties of $1 \times 10^{-4}$ g/cm$^3$ and $1 \times 10^{-2}$ mPa s in density and viscosity, respectively. The models were found to be in good agreement with the experimental values. The study highlights the importance of density and viscosity for quality control and engine performance of biofuels. The deveoped models for predicting the physical properties of green diesel and n-alkanes can be useful for quality control and optimization of biofuel production processes. The findings can be useful for researchers, engineers, and policymakers working in the field of biofuels and renewable energy. Further research is needed to explore the applicability of the developed models to other types of biofuels and to investigate the environmental and economic sustainability of green diesel production.

*Keywords:* Biofuel; green diesel; alkanes; density; viscosity; predictive models; physical properties.

DOI: https://doi.org/10.31349/RevMexFis.70.041701

## 1. Introduction

The depletion of fossil fuels is one of the key factors driving the search for new renewable energy sources. Fossil fuels such as coal, oil, and natural gas are finite resources that have been formed over millions of years and are being consumed at a much faster rate than they can be replenished. This means that eventually, these fuels will become scarce and more difficult to extract, leading to higher prices and potential supply shortages.

In addition to concerns about depletion, there is also growing awareness of the environmental impact of burning fossil fuels. The combustion of these fuels releases large amounts of greenhouse gas (GHG) emissions such as carbon dioxide into the atmosphere, contributing to global climate change. Renewable energy sources such as green diesel offer a potential solution to both challenges by providing a sustainable alternative to traditional fossil fuels with lower GHG emissions [1-4].

Researchers have estimated that by 2040, half of the energy sources used in the world will come from renewable sources [5]. Biomass is a renewable energy source that can be converted into liquid transportation fuels [6]. Increasing the use of biofuels (BF) in the transportation sector could contribute to reducing GHG emissions [7]. In addition, this benefits the diversification of energy sources, improved energy security, and stimulation of the rural agricultural economy [8]. Unlike petroleum diesel fuels, biofuels have the potential to reduce greenhouse gas emissions. Kalnes *et al*. reported that GHG emissions of green diesel (GD) were over 80% lower than those of petroleum diesel and approximately 40% lower than those of BD [9].

GD is a BF obtained from biomass conversion, which has properties like fossil diesel (FD) [10]. The chemical composition can vary depending on the technology and the raw material (biomass) used to produce it. Some of these technologies are commercial, while others are still in the research and development phase. In the realm of technologies, several noteworthy processes have been identified, including hydrodeoxygenation (HDO), pyrolysis, thermal hydrotreatment, and biomass-to-liquid (BTL) [11]. Similarly, various raw materials have been considered for these processes, such as wood, agro-industrial waste, animal fats (beef tallow, lard), and both recycled and virgin vegetable oils [12].

The HDO of vegetable oils or animal fats involves two reactions. In the first stage, triacyl glycerides react with hydrogen to produce a mixture of fatty acids and propane. In this step, there is hydrogenation of the double bonds between carbon and carbon. In the second stage, there are three simultaneous reactions, deoxygenation (DO), decarbonization (DCx), and decarbonization (DC), whereby oxygen is removed from fatty acids and n-alkanes are obtained as desirable products and by-products such as water ($H_2O$), carbon dioxide ($CO_2$) and carbon monoxide (CO) [13]. The triacylglyceride hydrotreatment process is versatile, as it allows the treatment of a variety of vegetable oils and fats.

At the industrial level, engineers commonly have conducted the HDO using heterogeneous catalysts such as

CoMo/$\gamma$-$Al_2O_3$, NiMo/$\gamma$-$Al_2O_3$, and Pd/$\gamma$-$Al_2O_3$ [14-18]. In the exploration of raw materials, an array of options is available, encompassing both vegetable and animal fats. Among these, vegetable oils stand out as the most widely employed, boasting a diverse range that comprises *jatropha*, sunflower, soybean, palm, and waste vegetable oil [15,19-22].

The main amount of actual GD is produced through hydrotreatment around the world and is characterized by having undesirable cold properties and poor lubricity [23]. Therefore, mixing it with fossil diesel is a frequent practice to eliminate the above problems. In cooperation with FD, GD represents a workable option to meet the world's demand for fuels. Unlike biodiesel (BD), which is a mixture of alkyl esters (methyl or ethyl esters), GD is produced up of hydrocarbons, and it is fully compatible with FD [24].

The characteristics of GD are as follows: (1) high product quality, (2) low content of aromatics, (3) low content of hetero compounds (such as oxygen, sulfur, or nitrogen), (4) high heat value, (5) high concentration of cetane [25,26].

The EN15940 standard represents an internationally recognized norm for GD (Gasoline and Diesel) fuel, which can be categorized as a paraffinic fuel. This class of fuel is known for its cleanliness and high quality, and it can be derived from a diverse range of processes, including gas-to-liquid (GTL) and hydrotreated vegetable oil (HVO). A notable advantage of paraffinic fuels is their fungibility, allowing for their seamless integration in both present and future diesel engines alongside fossil diesel in substantial concentrations. Consequently, these fuels can be efficiently distributed, stored, and utilized using existing infrastructure [27]. The paraffinic fuel specification EN15940 Class A has the following superior properties compared with conventional diesel, a higher cetane number, lower aromatics content, and lower sulfur content [27].

To the best of our knowledge, few works report the physical and chemical properties of GD. For example, Simacek *et al*. [28] reported the density and viscosity of GD obtained by hydrotreating rapeseed oil at a laboratory scale. In that study, the authors used temperatures between 583.15 to 633.15 K and pressures of 7 to 15 MPa. Furthermore, these authors used a commercial catalyst based on NiMo/$Al_2O_3$, and the reaction products obtained in that work contained mostly linear alkanes, especially n-heptadecane, and n-octadecane, as well as branched alkanes and other compounds in lower concentrations [28].

The GD quality as fuel is usually determined through its physical properties, such as viscosity, surface tension, density, latent heat of vaporization, thermal conductivity, heat capacity, boiling temperature, etc. [29,30].

Both density and viscosity are physical properties that play a significant role during the fuel injection and atomization processes [31]. The amount of fuel introduced into the combustion chamber per unit of time, known as the injection flow, can be estimated using equations of motion, where density is involved. If density increases, the injection flow decreases, causing partial combustion of the fuel, and increased smoke and particulate matter (PM) emissions, due to a worse atomization process [32].

Macroscopic and microscopic phenomena occur during the atomization process. The penetration of atomization is a macroscopic phenomenon due to two factors: the linear movement and the fuel viscosity of the injected fuel [33]. The diameter of the drop is a microscopic phenomenon in the atomization process.

As part of fuel quality, both density and viscosity are relevant properties to define mass transport. In addition, both properties are used during the design, operation, maintenance, and control of many processes.

The scarcity of experimental data and prediction models for GD highlights the need for further research in this area. By providing valuable information on the properties of GD, this study can contribute to a better understanding of its potential as a renewable energy source. Furthermore, our findings can help improve quality control measures for biofuels and enhance their performance in engines.

Considering the aforementioned factors, the density and dynamic viscosity of n-alkanes and GD will be subject to measurement with temperature variations. Moreover, efforts will be made to construct predictive models that can demonstrate a high degree of accuracy in estimating these specific physical properties.

## 2. Materials and methods

### 2.1. Vegetable oils

Refined palm and soybean oils were purchased from Interquímica S.A. de C.V. in Mexico City.

The fatty acids present in palm and soybean oils were indirectly determined through fatty acid methyl esters (FAMEs) of palm biodiesel. Palm and soybean oils were used to produce biodiesel samples by transesterification using methanol and potassium hydroxide, where the reaction was carried out at 60°C for four hours. The molar ratio of methanol: vegetable oil: catalyst used for the experiment was 60:10:2. The concentration of every FAME was determined and characterized by Gas-Chromatography-Mass-Spectroscopy (GC-MS). In the experimentation process, the gas chromatograph utilized was an HP Agilent 6890, accompanied by a selective mass detector (HP 5973), and a capillary column (HP-88). The capillary column, constructed from cyanopropyl polysiloxane (88 percent), possessed specific dimensions: 100 meters in length, an internal diameter of 0.25 mm, and a film thickness of 0.20 $\mu$m.

Chromatography procedures were executed with a detector temperature set at 250°C, an injection volume of 1.0 $\mu$L, a carrier gas (Helium) flow of 0.9 mL/min, and a split ratio of 50:1. The heating ramp employed was initiated at 80°C and maintained for three minutes, after which it increased at a rate of 4°C/min until reaching 250°C, where it was held steady for 15 minutes.

Additionally, measurements of the chemical and physical properties of palm and soybean oils were conducted within the laboratory setting. These measurements were carried out following specific methods, which encompassed elemental analysis (ASTM D5291 and ASTM D4629), density (ASTM D7042), flash point (ASTM D93), freezing point (ASTM D2386), and kinematic viscosity (ASTM D445).

### 2.2. Green diesel

Refined palm and soybean oils were used as feedstock in a micro plant to produce the GD.

Figure 1 offers a comprehensive visual depiction of the micro plant infrastructure, delineating its various sections that collectively facilitate its operations. The aforementioned sections encompass a) the mechanism responsible for introducing raw materials or substances into the system, b) the reactor in which chemical processes or transformations take place, and c) the unit designed to isolate and extract desired components or products from the reaction mixture. Each of these sections plays a crucial role in the overall functionality of the micro-plant, contributing to its efficiency and efficacy in carrying out specific tasks or processes within its intended domain.

Figure 1 shows graphically the predictive capacity of Eq. (4), where the surface represents the density estimations, while the black spheres correspond to the experimental values.

The procedure to obtain GD is the following. The vegetable oil was preheated at 333 K before being introduced into the process, and the feed flow was determined based on the weight difference of the loading container. The feedstock flows through the mini-plunger pump at the reactor operating pressure, joining with the high-purity hydrogen gas stream to pass to the reaction section.

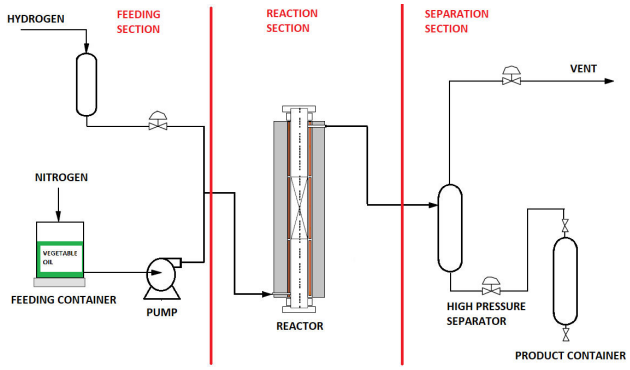


FIGURE 1. Microplant sections: a) feeding, b) reaction and c) separation.

TABLE I. Reactor operating conditions.

| Variable | Value |
|---|---|
| P, kPa | 4903 |
| T, K | 613 |
| SV, $s^{-1}$ | 3600 |
| $H_2$/HC ratio, $Nm^3/m^3$* | 935 |

*Normal cubic meter per cubic meter (The normal condition is given at a temperature of 293.15 K and absolute pressure of 101.3 kPa).

All lines from the suction and discharge of the mini-dosing pump are heated to keep the load fluid, and thus avoid plugging because of cold spots.

The nitrogen stream was used to keep the pressure in the loading container, providing stability to the flow of the liquid feed and keeping the head for the correct operation of the mini-dosing pump. Fed fresh hydrogen flow from the cylinder to the storage tank for the hydrogen gas supply, controlling the pressure of the hydrogen through a pressure regulator.

The reaction section comprises a fixed bed of 15 ml of catalyst. The vegetable oil and the fresh hydrogen gas are mixed into the reactor at 4903 kPa and 613 K. The reactor has three temperature control loops through electrical resistances. The reaction of vegetable oil with hydrogen occurs on the outer and inner surfaces of the catalyst pores. The reaction products exit the top of the reactor and flow to the separation section.

The HDO of the vegetable oil was performed using a NiMo/$TiO_2$ -$\gamma$-$Al_2O_3$ catalyst loaded in a fixed bed reactor under the operating conditions reported in Table I.

The catalyst was characterized by different techniques. From the physisorption test, it was obtained that the catalyst had a surface area of 188 $m^2$/g, a total pore volume of 0.47 $cm^3$/g, and an average pore diameter of 70 angstroms. From the atomic adsorption test, it was found that the metallic content in the catalyst is 11.5 wt% of molybdenum, 2.9 wt% of nickel, 5.6 wt% of titanium, and less than 0.01 wt% of sodium.

X-ray diffraction (XRD) analysis showed the characteristic reflections of titania in its anatase phase. It is important to highlight that the nickel content is crucial in this catalyst as it promotes hydrogenation reactions, facilitating the cleavage of chemical bonds in oxygenated compounds during hydroprocessing, resulting in deoxygenation.

The nickel content also affects the stability and durability of the catalyst during the hydroprocessing process. An optimal concentration of nickel is able to sustain the catalytic functionality and structural coherence of the catalyst over extended durations, whereas excessively elevated or diminished levels may result in untimely deterioration.

Although the NiMo/$TiO_2$-g-$Al_2O_3$ catalyst was used in this study, it is important to note that other types of catalysts are available, using different supports such as $Al_2O_3$, $TiO_2$, $ZrO_2$, $SiO_2$, mesoporous materials like HMS, SBA-15, KIT-6, MCM-41, mixed oxides like $Al_2O_3$-$TiO_2$, $TiO_2$-$SiO_2$, $TiO_2$-$ZrO_2$, $SiO_2$-$Al_2O_3$, $ZrO_2$-$SiO_2$, and zeolites like NaY, USY, Beta, ZSM-5. Additionally, various active metals have been employed including nickel, cobalt, molybdenum, tungsten, iron, and noble metals. However, the most widely

used catalysts for the hydrodeoxygenation of vegetable oils are nickel-molybdenum supported on alumina [34].

The reaction mechanism for HDO comprises two stages. First, hydrogenation of double bonds occurs, as well as cleavage of the C-O bond, obtaining diacylglycerides, monoglycerides, carboxylic acids, and propane. Second, the conversion of carboxylic acids to n-alkanes occurs through three parallel reactions: DO, DCx, and DC. The DO reaction yields alkanes and $H_2O$, while the DCx reaction enables the production of alkanes and $CO_2$. Lastly, the DC reaction results in the generation of alkanes, $H_2O$, and CO.

The reaction products and the unreacted hydrogen reach the high-pressure separator, where the separation of the gas and liquid products occurs at the top and bottom.

The gaseous product was quantified using a meter-totalizer and chromatography. The excess gaseous product passes through an acid gas neutralizer and subsequently to a gas burner. The liquid product, a mixture of GD and $H_2O$, is sent to a container to be accumulated and analyzed.

The hydrocarbon composition of GD was analyzed using the chromatograph. For the separation of paraffinic compounds, a capillary column (DB-1HT) was employed, con-

TABLE II. Vegetable oil properties.

| Fatty acid | Abbreviation | PO ,wt% | SO ,wt% |
|---|---|---|---|
| Octanoic Acid | C8:0 | 0.01 | 0.17 |
| Dodecanoic Acid | C12:0 | 0.57 | 0 |
| Tetradecanoic Acid | C14:0 | 2.5 | 0.28 |
| Pentadecanoic Acid | C15:0 | 0.09 | 0.04 |
| Hexadecanoic Acid | C16:0 | 39.22 | 17.47 |
| 9-Hexadecenoic Acid | C16:1 | 0.55 | 0.07 |
| (9Z,12Z)-Hexadeca-9-12-dienoic Acid | C16:2 | 0 | 0.03 |
| Heptadecanoic Acid | C17:0 | 0.29 | 0.11 |
| Cis-9-Heptadecenoic | C17:1 | 0.09 | 0.34 |
| Octadecanoic Acid | C18:0 | 4 | 3.9 |
| 9-Octadecenoic Acid (Z) | C18:1 | 36.55 | 25.1 |
| (9Z,12Z)-Octadeca-9-12-dienoic Acid | C18:2 | 12.38 | 38 |
| (9Z, 12Z, 15Z)-Octadeca-9,12,15-trienoic Acid | C18:3 | 1.19 | 10.3 |
| Eicosanoic Acid | C20:0 | 1.05 | 1.09 |
| Cis-11-Eicosenoic Acid | C20:1 | 0.56 | 0.64 |
| Cis-11,14-Eicosadienoic Acid | C20:2 | 0 | 0.19 |
| Docosanoic Acid | C22:0 | 0 | 1.13 |
| Tricosanoic Acid | C23:0 | 0 | 0.18 |
| Ricinoleic Acid | C18:1 OH | 0 | 0.24 |
| Tetracosanoic Acid | C24:0 | 0 | 0.46 |
| Pentacosanoic Acid | C25:0 | 0 | 0.13 |
| Hexacosanoic Acid | C26:0 | 0 | 0.07 |
| Others | - | 0.95 | 0.06 |
| Atoms from Elemental Analysis | Units | PO | SO |
| C | $wt\%$ | 74.99 | 76.85 |
| H | $wt\%$ | 12.51 | 11.59 |
| O | $wt\%$ | 12.5* | 11.56* |
| N | mg/kg | 3.2 | 2.2 |
| Physical Properties | Units | PO | SO |
| Density at 20°C | g/cm$^3$ | 0.9112 | 0.9208 |
| Viscosity at 40°C | mm$^2$/s | 40.66 | 30.8 |
| Flash Point | °C | 332 | 348 |
| Pour Point | °C | 9 | -6 |
| Cloud Point | °C | 19 | -5 |
| Water and Sediments | vol% | 0.3 | 0 |

PO = Palm Oil, SO = Soybean Oil.

sisting of a dimethylpolysiloxane phase at 100%, and featured the following dimensions: 30 meters in length, an internal diameter of 0.32 mm, and a film thickness of 0.10 $\mu$m. Standard n-alkanes ranging from $C_{10}$ to $C_{25}$ were used as a reference mixture.

The detector temperature was set at 250°C, and a sample volume of 1 mL was injected into the chromatograph. Helium was utilized as the carrier gas with a flow rate of 0.023 $cm^3/s$, while the split ratio was maintained at 50:1. The heating ramp initiated at 80°C for five minutes, after which the column temperature was elevated to 250°C at a heating rate of 6 °Cmin. Finally, the temperature of 250°C was held steady for 15 minutes.

### 2.3. Statistical parameters

Three statistical parameters were employed to assess the predictive capability of the empirical correlations for density and viscosity. These parameters included the average absolute deviation $AAD$, correlation coefficient $R$, and standard deviation $\sigma$, which could be estimated using the following Eqs. (1)-(3).

$$AAD = \frac{\sum_{i=1}^{n} \left( \left| \frac{(f_{\exp,i} - f_{\text{cal},i}) \times 100}{f_{\exp,i}} \right| \right)}{n}, \quad (1)$$

where $n$ is the number of experimental or calculated points, $f$ is the physical property, and $AAD$ is the average absolute deviation expressed in percent.

$$R = \frac{\sum_{i=1}^{n} \left( f_{\exp,i} - \bar{f_{\exp}} \right) \left( f_{\text{cal},i} - \bar{f_{\text{cal}}} \right)}{\sqrt{\sum_{i=1}^{n} \left( f_{\exp,i} - \bar{f_{\exp}} \right)^2 \sum_{i=1}^{n} \left( f_{\text{cal},i} - \bar{f_{\text{cal}}} \right)^2}}, \quad (2)$$

where $\bar{f}$ is the surface tension average, and $R$ is the dimensionless correlation coefficient. If $R$ is near unity is a sign that the model has good accuracy.

$$\sigma = \sqrt{\frac{\sum_{i=1}^{n} \left( f_{\exp} - f_{\text{cal}} \right)^2}{n - m}}, \quad (3)$$

where $\sigma$ is the standard deviation, $n$ is the number of experimental points, and $m$ is the number of parameters.

## 3. Results and discussion

### 3.1. Vegetable oils properties

Table II shows the fatty acid composition of the refined palm and soybean oils measured in this work and the physical and chemical properties of this vegetable oil. The measurements of these properties were conducted in laboratories affiliated with the Mexican Petroleum Institute.

Among the fatty acids present in refined palm oil, hexanoic, 9-octadecanoic, and (9Z,12Z)-octadeca-9-12-dienoic acids exhibited higher concentrations, while in refined soybean oil, hexanoic, 9-octadecanoic, (9Z,12Z)-octadeca-9-12-dienoic, and (9Z,12Z,15Z)-octadeca-9-12-15-trieonic acids were present in major proportions.

The elemental analysis revealed that the oxygen concentration in refined palm oil was 12.5 wt%, and in refined soybean oil, it was 11.5 wt%. Notably, this oxygen concentration was determined through a difference-based approach.

The error in determining the concentration of fatty acids was measured at 0.01 weight percent. The error of the remaining properties listed in Table II adhered to ASTM standards. Such as ASTM D5291 for the determination of carbon, hydrogen, and nitrogen atom concentrations, ASTM D7042 for density, ASTM D93 for flash point, ASTM D2386 for freezing point, and ASTM D445 for kinematic viscosity. These standards were utilized to ensure repeatability in the experimental measurements. Every ASTM standard provides its own correlation to calculate the reproducibility.

### 3.2. GD properties

GD is mainly composed of linear n-alkanes from $C_8$ to $C_{20}$ (Table III). The rest belong to cycloalkanes, branched alkanes, and aromatics. The concentration and type of n-alkanes varied depending on the following factors: (a) the catalyst, (c) the operating conditions used for the hydrodeoxygenation process (Table I), (b) the fatty acid composition of the palm and soybean oils (Table II).

The compounds present in higher concentrations were n-alkanes $C_{15}$ to $C_{18}$, which agree with the type of carboxylic acid present in the palm and soybean oils in higher concentrations (palmitic, stearic, oleic, and linoleic acids).

Table IV summarizes the physical and chemical properties of GD. A comparison was made between these properties and the specifications outlined in the NOM-016-CRE-2016 Mexican standard for FD [35]. Table IV also includes the EN 15940:2016 standard specifications for the fuel obtained by the hydrotreated vegetable oil (HVO) process [36] and the ASTM D975 standard specifications for a fossil diesel [37].

### 3.3. Prediction of n-alkanes and GD density

Initially, information from experimental data present in the literature concerning the density variation of n-alkane with temperature [38] was sought and retrieved. Subsequently, correlations were derived from this gathered information to predict the property in two distinct approaches. The first involved estimating the density as a function of temperature for each n-alkane, while the second utilized mathematical expressions where the property was determined based on molecular weight and fixed temperature.

To validate the derived predictions, the Rackett equation was employed to calculate the density of the n-alkanes [39]. The results of these calculations have been included in the supplementary material for reference.

To establish a comprehensive and generalized model, a correlation was derived, wherein the density was formulated as a simultaneous function of both temperature and the

TABLE III. Vegetable oil properties.

| Compound | Retention Time | Abbreviation | GD-PO,wt% | GD-SO, wt% |
|---|---|---|---|---|
| Nonane | 2.194 | C9 | 0 | 0.01 |
| Decane | 3.251 | C10 | 0 | 0.12 |
| Undecane | 5.143 | C11 | 0.1 | 0.23 |
| Dodecane | 7.989 | C12 | 0.19 | 0.25 |
| Tridecane | 11.549 | C13 | 0.64 | 0.26 |
| Tetradecane | 15.444 | C14 | 1.07 | 0.23 |
| Pentadecane | 19.492 | C15 | 20.12 | 8 |
| Hexadecane | 23.48 | C16 | 34.13 | 8.6 |
| Heptadecane | 28.267 | C17 | 25.54 | 42.24 |
| Octadecane | 31.881 | C18 | 17.71 | 35.04 |
| Nonandecane | 34.238 | C19 | 0 | 1.18 |
| Eicosane | 37.236 | C20 | 0 | 0.77 |
| Heneicosane | 39.532 | C21 | 0 | 0.65 |
| Docosane | 41.291 | C22 | 0 | 0.13 |
| Other | - | - | 0.5 | 2.29 |

GD-P0 = Green diesel from palm oil, GD-SO = Green diesel from soybean oil.

molecular weight of the n-alkanes. The resulting equation is denoted as Eq. (4).

$$\rho = 0.9694 - 0.0024\,T + 0.000317\,T\ln(W). \qquad (4)$$

Here, $\rho$ is the density in g/cm$^3$, $T$ is the temperature in $K$, and $W$ is the molecular weight in g/mol.

The estimates obtained demonstrated a high level of accuracy as the predictions closely aligned with the experimental data, resulting in an $AAD$, $R$, and $\sigma$ of 0.31%, 0.9968, and 0.0027 g/cm$^3$, respectively.

Figure 2 shows graphically the predictive capacity of Eq. (4), where the surface represents the density estimations, while the black spheres correspond to the experimental values.

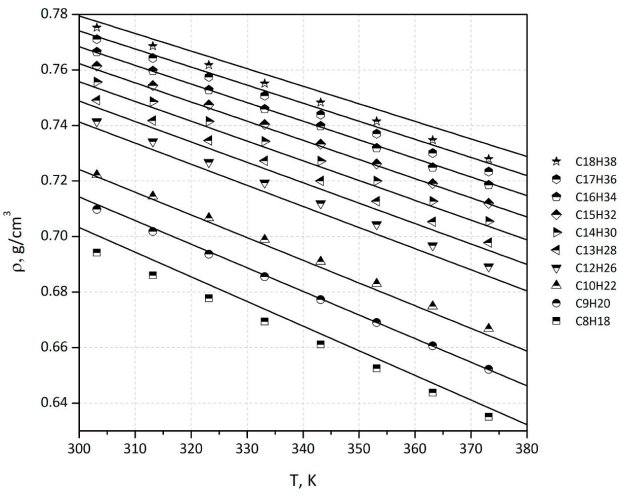


FIGURE 2. Density of n-alkanes ($C_8$ to $C_{18}$).

On the other hand, the experimental densities of GD were determined over a temperature range spanning from 303.15 K to 373.15 K. The experimental results were between 0.7195 to 0.7687 g/cm$^3$ in the case of GD derived from palm oil and 0.6999 to 0.7460 g/cm$^3$ in the case of GD derived from soybean oil, as seen in Table V. The density error indicated in Table V stood at 0.0001 g/cm$^3$.

The results of the gas chromatography analysis showed that the concentration of n-alkanes in the GD was about 99.5 weight% (Table III), while the remaining correspond to traces of cycloalkanes, branched alkanes, and aromatics.

The density of GD was estimated utilizing Eq. (5), employing the mixing rule proposed by Kay [40]. For the estimation, binary interaction terms were omitted, given the assumption that GD primarily consists of a mixture of n-alkanes, resembling the behavior of an ideal solution. An additional term was introduced to the Kay model, serving as a correction factor associated with the presence of components present in smaller quantities, such as cycloalkanes, branched alkanes, and aromatics.

$$\rho_{GD} = \sum_{i=1}^{n} x_i\,\rho_i + CF, \qquad (5)$$

where $\rho_{GD}$ is the density of GD, *i* is a subscript that refers to all alkanes, $x$ is the mole fraction, and *CF* is the contribution to the global density of cycloalkanes, branched alkanes, and aromatics.

Equation (6) was used to estimate the mol fraction $x_i$ for each alkane from its mass fraction $w_i$.

$$x_i = \frac{\frac{w_i}{W_i}}{\sum_{i=1}^{n}\frac{w_i}{W_i}}. \qquad (6)$$

TABLE IV. Physical and chemical properties of GD.

| Property | ASTM | GD-PO | GD-SO | $NOM016$ | $EN15940$ | $ASTMD975$ |
|---|---|---|---|---|---|---|
| Flash point, °C | D93 | 136 | 142 | $> 45$ | $> 55$ | $> 52$ |
| Kinematic viscosity at 40°C, $mm^2/s$ | D7042 | 2.978 | 3.477 | 1.9-4.1 | 2-4.5 | 1.9-4.1 |
| Distillation Temp. at 90 vol%, °C | D86 | 320 | 323 | $< 345$ | $< 360$ | $< 338$ |
| Cetane index | D976 | 74.7 | 80.9 | $> 45$ | * | $> 40$ |
| Sulfur, mg/kg | D5453 | 1.223 | 0.073 | $< 500$ | $< 5$ | $< 15$ |
| Aromatics, vol% | D1319 | 2.2 | 3.8 | $< 35$ | ** | $< 35$ |

GD-P0 = Green Diesel from Palm Oil; GD-SO = Green Diesel from Soybean Oil;
*The EN 15940:2016 standard specifies a cetane number $> 70$ for the paraffinic fuel obtained by HVO;
**The EN 15940: 2016 standard specifies a total aromatic content $< 1.1$ by weight for paraffinic compounds obtained by HVO.

TABLE V. Experimental and calculated density of GD expressed in $g/cm^3$ at various temperatures.

| | | $T, K$ | | | | | | | |
|---|---|---|---|---|---|---|---|---|---|
| Biofuel | Value Type | 303.15 | 313.15 | 323.15 | 333.15 | 343.15 | 353.15 | 363.15 | 373.15 |
| GD-PO | Exp. | 0.7687 | 0.7622 | 0.7556 | 0.749 | 0.7422 | 0.735 | 0.7271 | 0.7195 |
| GD-PO | Cal. | 0.7685 | 0.7619 | 0.7549 | 0.7483 | 0.7416 | 0.7348 | 0.7282 | 0.7215 |
| GD-SO | Exp. | 0.7460 | 0.7391 | 0.7337 | 0.7260 | 0.7209 | 0.7139 | 0.7064 | 0.6999 |
| GD-SO | Cal. | 0.7458 | 0.7394 | 0.7330 | 0.7268 | 0.7204 | 0.7142 | 0.7075 | 0.7013 |

It is important to note that the density of n-alkanes can be estimated using Eq. (4). This estimation can then be utilized to derive an estimate of the density of GD by substituting Eq. (4) in Eq. (5), leading to the formulation of Eq. (7).

$$\rho_{GD} = \sum_{i=1}^{n} x_i \Big[ 0.9694 - 0.0024\, T + 0.000317\, T \ln(W_i) \Big] + 0.00825. \qquad (7)$$

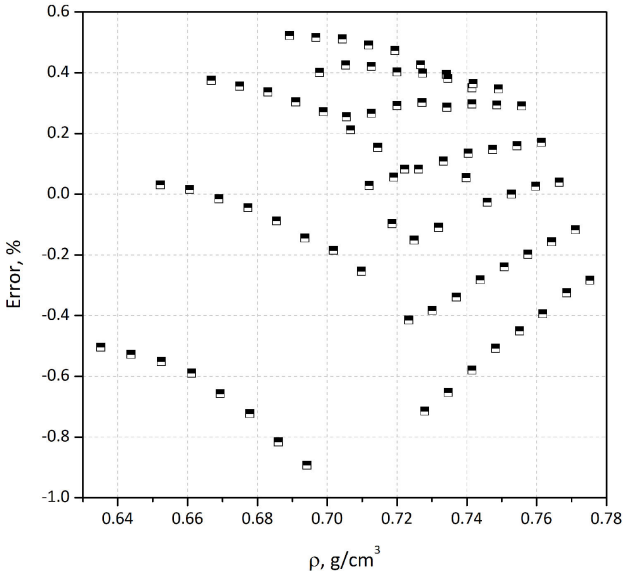


FIGURE 3. The relative error in the prediction of the density of n-alkanes ($C_8$ to $C_{18}$).

The value of $CF$ (0.00825) was obtained using the generalized reduced gradient (GRG) method, employing the experimental density of GD obtained in this study. The predictions of Eq. (7) were good because an $AAD$ of 0.1% was obtained when both green diesels derived from palm and soybean oil were compared.

### 3.4. Prediction of n-alkanes and dynamic viscosity

This section presents the results obtained in the prediction of the dynamic viscosity of n-alkanes and GD.

In 2011, Ramírez-Verduzco *et al*. proposed correlations to predict the viscosity of methyl esters and biodiesel [41]. Subsequently, a comparable method was pursued to estimate the dynamic viscosity of both n-alkanes and GD. The procedure comprises changing the last mathematical term of the equation proposed by Krisnangkura [42] [Eq. (8)], the modification was the replacement of $\lambda(W/T)$ by $\lambda(W/T)^2$ to obtain the Eq. (9),

$$\mu = \exp\left( \ln(\gamma) + \frac{\omega}{T} + \varphi\, W + \lambda \frac{W}{T} \right), \qquad (8)$$

$$\mu = \exp\left( \ln(\gamma) + \frac{\omega}{T} + \varphi\, W_i + \lambda \frac{W}{T^2} \right), \qquad (9)$$

where $\mu$ is the dynamic viscosity, $T$ is the temperature, $W$ is the molecular weight, and $\gamma$, $\omega$, $\phi$, and $\lambda$ corresponds to the adjusted parameters.

The experimental data on the dynamic viscosity of the n-alkanes from the literature [38] were utilized to determine

TABLE VI. Experimental and calculated dynamic viscosity of GD expressed in *m*Pa s at various temperatures.

| | | $T, K$ | | | | | | | |
|---|---|---|---|---|---|---|---|---|---|
| Biofuel | Value Type | 303.15 | 313.15 | 323.15 | 333.15 | 343.15 | 353.15 | 363.15 | 373.15 |
| GD-PO | Exp. | 2.77 | 2.27 | 1.86 | 1.51 | 1.34 | 1.18 | 1.02 | 0.875 |
| GD-PO | Cal. | 2.86 | 2.30 | 1.88 | 1.56 | 1.31 | 1.12 | 0.96 | 0.83 |
| GD-SO | Exp. | 03.16 | 2.57 | 2.09 | 1.79 | 1.42 | 1.29 | 1.09 | 0.88 |
| GD-SO | Cal. | 3.26 | 2.60 | 2.11 | 1.74 | 1.45 | 1.23 | 1.05 | 0.91 |

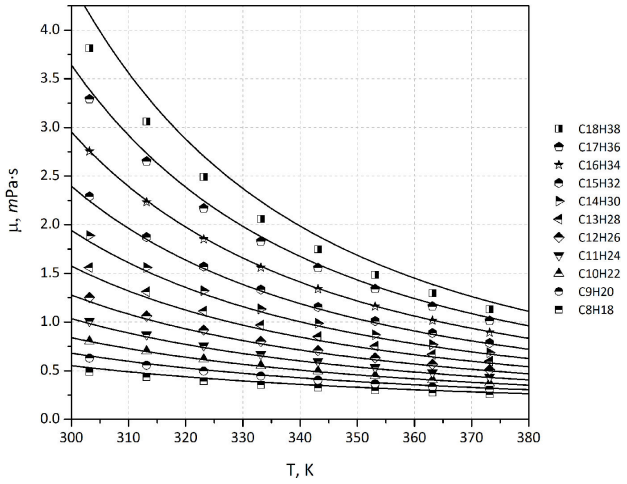


FIGURE 4. Dynamic viscosity of n-alkanes ($C_8$ to $C_{18}$).

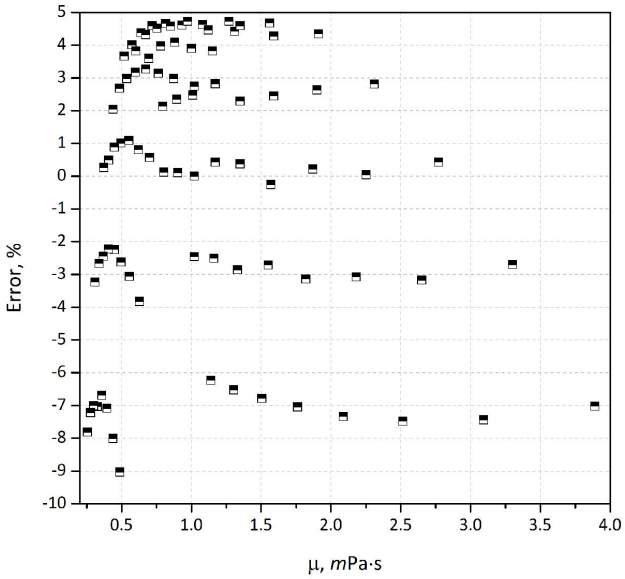


FIGURE 5. The relative error in the prediction of the dynamic viscosity of n-alkanes ($C_8$ to $C_{18}$).

fixed parameters ln($\gamma$), $\omega$, $\phi$, and $\lambda$ in Eq. (9) which allowed the derivation of Eq. (10). The adjustment of coefficients was performed using the Levenberg-Marquardt algorithm [43].

$$\mu = \exp\left(-3.261 + \frac{288.1}{T} + 0.002 + 1121.97\frac{W}{T^2}\right). \quad (10)$$

Upon comparing the predictions generated using Eq. (10) with the experimental data, the following statistical parameters were obtained: $AAD$, $R$, and $\sigma$ of 3.6%, 0.9979, and 0.062 mPa s, respectively.

Figure 4 shows the graphical comparison between the experimental results (symbols) and those estimated by Eq. (10) (curved lines).

Figure 5 shows the relative error obtained with Eq. (10), which was between -9 and 4.7%.

Various mathematical arrangements were examined to establish correlations between the dynamic viscosity of n-alkanes and its dependency on $T$ and $W$. These alternative correlations have been provided in the supplementary material. However, it was observed that the correlation expressed by Eq. (10) exhibited the most accurate predictive capability. About the experimental results for the dynamic viscosity of GD, obtained over a temperature range from 303.15 K to 373.15 K, values were recorded between 0.899 to 2.775 mPa s for GD derived from palm oil.

These values corresponded to the higher and lower temperatures, respectively, as listed in Table VI. Notably, it is evident from the data that the viscosity decreases with increasing temperature. It is notable to mention that the experimental uncertainty in viscosity amounted to 0.01 mPa s.

The GD viscosity estimated through Eq. (11) contains two terms. The first term is the mixing rule proposed by Grunberg-Nissan [44], where the binary interaction contribution was negligible. In this context, it is considered that GD exhibits behavior close to that of an ideal solution due to its composition, predominantly consisting of n-alkanes with similar molecular weights. The second term present in Eq. (11) serves as a correction factor proposed for GD, accounting for its minor presence of cycloalkanes, branched alkanes, and aromatics.

$$\ln \mu_{GD} = \sum_{i=1}^{i=n} x_i \ln\ \mu_i + CF. \quad (11)$$

Upon substituting Eq. (10) in Eq. (11), Eq. (12) is obtained.

$$\rho_{GD} = \sum_{i=1}^{n} x_i \big[0.9694 - 0.0024\,T + 0.000317\,T \ln\left(W_i\right)\big] + 0.00825. \quad (12)$$

The correction factor of $-0.114$ included in Eq. (12) was estimated using the nonlinear GRG method. An $AAD$ of 3.1% was observed in dynamic viscosity when comparing both green diesels derived from palm and soybean oil.

## 4. Conclusions

This study investigated the density and dynamic viscosity of GD produced from palm and soybean oils hydrotreatment and developed models to predict the physical properties of GD and n-alkanes. The density of GD was found to be slightly higher than that of traditional fossil diesel, while its viscosity was lower. The developed models were found to be in good agreement with the experimental values and can be useful for quality control and optimization of biofuel production processes.

Given the significance of GD in meeting global demand for environmentally friendly fuels. A comprehensive production and characterization process was undertaken, involving the conversion of palm and soybean oils into GD. Rigorous assessments of various chemical and physical properties, adhering to ASTM standards, were conducted in this characterization. Our findings confirmed the high quality of the produced GD, predominantly composed of n-alkanes ranging from $C_8$ to $C_{20}$. As a result, GD can effectively substitute fossil diesel in engines, contributing to cleaner energy solutions.

Acknowledging the pivotal roles that density and viscosity play in process design, operation, and engine performance, the density and dynamic viscosity of n-alkanes and GD were precisely measured experimentally during this study, achieving uncertainties of $1 \times 10^{-4}$ g/cm$^3$ and $1 \times 10^{-2}$ mPa s, respectively. Additionally, empirical correlations were developed to predict the mentioned thermodynamic properties of both n-alkanes and GD, considering the influence of temperature and molecular weight on their density and viscosity. In the case of GD, we incorporated the mixing rules proposed by Kay and Grumberg-Nissan, utilizing the composition and physical properties as inputs for the models. To account for the minor presence of cycloalkanes, branched alkanes, and aromatics in GD, a correction term was included in these models. Notably, our models successfully predicted these physical properties, exhibiting strong agreement with the experimental data. The above models can be useful for the quality control of biofuels and can be successfully incorporated into process simulators.

The study highlights the importance of density and viscosity for quality control and engine performance of biofuels. The findings can be useful for researchers, engineers, and policymakers working in the field of biofuels and renewable energy. Further research is needed to explore the applicability of the developed models to other types of biofuels and to investigate the environmental and economic sustainability of GP production.

The results suggest that GD has the potential as a biofuel with certain advantages over traditional fossil diesel. The developed models can be useful for predicting the physical properties of GD and n-alkanes, ultimately contributing to the optimization and quality control of biofuel production processes.

The models, although initially developed for a specific precursor oil, can be adapted for use with vegetable oils of different compositions. Through adjustments and calibration, their applicability extends to various types of precursor oils. This versatility allows for broader exploration and understanding across different oil types, facilitating insights and predictive capabilities useful in diverse industrial and research applications.

## Acknowledgments

We extend our sincere appreciation to the Instituto Mexicano del Petróleo for their generous financial support provided through Project D.62020. Gratitude is also expressed to Dra. Myriam Amezcua for her valuable insights on sustainability matters, and to Dr. Jorge Aburto for fostering research endeavors in the field of biofuels.

1. A. Kalair, *et al.*, Role of energy storage systems in energy transition from fossil fuels to renewables, *Energy Storage* **3** (2021), https://doi.org/10.1002/est2.135.
2. S. Shafiee and E. Topal, When will fossil fuel reserves be diminished?, *Energy Policy* **37** (2009) 181, https://doi.org/10.1016/j.enpol.2008.08.016.
3. N. Abas, A. Kalair, and N. Khan, Review of fossil fuels and future energy technologies, *Futures* **69** (2015) 31, https://doi.org/10.1016/j.futures.2015.03.003.
4. R. Bentley, Global oil and gas depletion: an overview, *Energy Policy* **30** (2002) 189, https://doi.org/10.1016/S0301-4215(01)00144-6.
5. F. Battaglia, Review of Gasoline, Diesel and Ethanol Biofuels from Grasses and Plants, *AIAA Journal* **49** (2011) 448, https://doi.org/10.2514/1.52159.
6. G. P. Towler, A. R. Oroskar, and S. E. Smith, Development of a sustainable liquid fuels infrastructure based on biomass, *Environmental Progress* **23** (2004) 334, https://doi.org/10.1002/ep.10052.
7. E. Smeets *et al.*, The impact of the rebound effect of the use of first generation biofuels in the EU on greenhouse gas emissions: A critical review, *Renewable and Sustainable Energy Reviews* **38** (2014) 393, https://doi.org/10.1016/j.rser.2014.05.035.
8. H. Gorter and D. R. Just, The Social Costs and Benefits of Biofuels: The Intersection of Environmental, Energy and Agri-

cultural Policy, *Applied Economic Perspectives and Policy* **32** (2010) 4, https://doi.org/10.1093/aepp/ppp010.

9. T. Kalnes, T. Marker, and D. R. Shonnard, Green Diesel: A Second Generation Biofuel, *International Journal of Chemical Reactor Engineering* **5** (2007), https://doi.org/10.2202/1542-6580.1554.

10. A. Demirbas, Relationships derived from physical properties of vegetable oil and biodiesel fuels, *Fuel* **87** (2008) 1743, https://doi.org/10.1016/j.fuel.2007.08.007.

11. S. L. Douvartzides *et al.,* Green Diesel: Biomass Feedstocks, Production Technologies, Catalytic Research, Fuel Properties and Performance in Compression Ignition Internal Combustion Engines, *Energies* **12** (2019) 809, https://doi.org/10.3390/en12050809.

12. A. S. Zaky, S. Kumar, and A. J. Welfle, Integrated Approaches and Future Perspectives (Springer International Publishing, 2022), pp. 613-651, https://doi.org/10.1007/978-3-030-91570-4_20.

13. M. Plazas-González, C. A. Guerrero-Fajardo, and J. R. Sodré, Modelling and simulation of hydrotreating of palm oil components to obtain green diesel, *Journal of Cleaner Production* **184** (2018) 301, https://doi.org/10.1016/j.jclepro.2018.02.275.
1

14. Y. Liu *et al.,* Hydrotreatment of Vegetable Oils to Produce Bio-Hydrogenated Diesel and Liquefied Petroleum Gas Fuel over Catalysts Containing Sulfided Ni-Mo and Solid Acids, *Energy and Fuels* **25** (2011) 4675, https://doi.org/10.1021/ef200889e.

15. B. Veriansyah *et al*., Production of renewable diesel by hydroprocessing of soybean oil: Effect of catalysts, *Fuel* **94** (2012) 578, https://doi.org/10.1016/j.fuel.2011.10.057.

16. J. Hancsók *et al*., Production of bioparaffins by the catalytic hydrogenation of natural triglycerides, *Journal of Cleaner Production* **34** (2012) 76, https://doi.org/10.1016/j.jclepro.2012.01.036.

17. A. T. Madsen *et al*., Hydrodeoxygenation of waste fat for diesel production: Study on model feed with Pt/alumina catalyst, *Fuel* **90** (2011) 3433, https://doi.org/10.1016/j.fuel.2011.06.005.

18. T. Morgan *et al.,* Catalytic deoxygenation of triglycerides to hydrocarbons over supported nickel catalysts, *Chemical Engineering Journal* **189-190** (2012) 346, https://doi.org/10.1016/j.cej.2012.02.027.

19. K.Murata *et al*., Production of Synthetic Diesel by Hydrotreatment of Jatropha Oils Using Pt-Re/H-ZSM-5 Catalyst, *Energy and Fuels* **24** (2010) 2404, https://doi.org/10.1021/ef901607t.

20. P. Šimáček *et al*., Premium quality renewable diesel fuel by hydroprocessing of sunflower oil, *Fuel* **90** (2011) 2473, https://doi.org/10.1016/j.fuel.2011.03.013.

21. A. Guzman *et al*., Hydroprocessing of crude palm oil at pilot plant scale, *Catalysis Today* **156** (2010) 38, https://doi.org/10.1016/j.cattod.2009.11.015.

22. S. Bezergianni *et al*., Hydrotreating of waste cooking oil for biodiesel production. Part I: Effect of temperature on product yields and heteroatom removal, *Bioresource Technology* **101** (2010) 6651, https://doi.org/10.1016/j.biortech.2010.03.081.

23. A. Vonortas and N. Papayannakos, Comparative analysis of biodiesel versus green diesel, Wiley Interdisciplinary Reviews: *Energy and Environment* **3** (2014) 3, https://doi.org/10.1002/wene.78.

24. N. Arun, R. V. Sharma, and A. K. Dalai, Green diesel synthesis by hydrodeoxygenation of bio-based feedstocks: Strategies for catalyst design and development, *Renewable and Sustainable Energy Reviews* **48** (2015) 240, https://doi.org/10.1016/j.rser.2015.03.074.

25. Y. Liu *et al*., Hydrotreatment of Jatropha Oil to Produce Green Diesel over Trifunctional Ni-Mo/SiO <sub>2</sub> -Al <sub>2</sub> O <sub>3</sub> Catalyst, *Chemistry Letters* **38** (2009) 552, https://doi.org/10.1246/cl.2009.552.

26. D. Tuli and S. Kasture, Biodiesel and green diesel (Elsevier, 2022), pp. 119-133, https://doi.org/10.1016/B978-0-323-88427-3.00010-6.

27. J. Rodríguez-Fernández *et al.,* Selection of Blends of Diesel Fuel and Advanced Biofuels Based on Their Physical and Thermochemical Properties, *Energies* **12** (2019) 2034, https://doi.org/10.3390/en12112034.

28. P. Šimáček *et al.,* Fuel properties of hydroprocessed rapeseed oil, *Fuel* **89** (2010) 611, https://doi.org/10.1016/j.fuel.2009.09.017.

29. S. Bezergianni and A. Dimitriadis, Comparison between different types of renewable diesel, *Renewable and Sustainable Energy Reviews* **21** (2013) 110, https://doi.org/10.1016/j.rser.2012.12.042.

30. D. Singh, K. Subramanian, and S. Singal, Emissions and fuel consumption characteristics of a heavy duty diesel engine fueled with Hydroprocessed Renewable Diesel and Biodiesel, *Applied Energy* **155** (2015) 440, https://doi.org/10.1016/j.apenergy.2015.06.020.

31. R. K. Pandey, A. Rehman, and R. Sarviya, Impact of alternative fuel properties on fuel spray behavior and atomization, *Renewable and Sustainable Energy Reviews* **16** (2012) 1762, https://doi.org/10.1016/j.rser.2011.11.010.

32. J. W. Hwang *et al.,* Effect of Fuel Injection Rate on Pollutant Emissions in DI Diesel Engine, Tech. rep., *SAE Technical Paper* (1999), https://doi.org/10.4271/1999-01-0195.

33. A. Demirbas and K. Dincer, Sustainable Green Diesel: A Futuristic View, Energy Sources, *Part A: Recovery, Utilization, and Environmental Effects* **30** (2008) 1233, https://doi.org/10.1080/15567030601082829.

34. N. Arun, R. V. Sharma, and A. K. Dalai, Green diesel synthesis by hydrodeoxygenation of bio-based feedstocks: Strategies for catalyst design and development, *Renewable and Sustainable Energy Reviews* **48** (2015) 240, https://doi.org/ https://doi.org/10.1016/j.rser.2015.03.074.

35. J. Koupal and C. Palacios, Impact of new fuel specifications on vehicle emissions in Mexico, *Atmospheric Environment* **201** (2019) 41, https://doi.org/10.1016/j.atmosenv.2018.12.028.

36. S. R. Chia *et al.,* Renewable diesel as fossil fuel substitution in Malaysia: A review, *Fuel* **314** (2022) 123137, https://doi.org/10.1016/j.fuel.2022.123137.

37. B. R. Moser, Impact of fatty ester composition on low temperature properties of biodiesel-petroleum diesel blends, *Fuel* **115** (2014) 500, https://doi.org/10.1016/j.fuel.2013.07.075.

38. N. Vargaftik, Handbook of physical properties of liquids and gases - pure substances and mixtures, Second edition ed. (Hemisphere Publishing Corporation, New York, NY, 1975).

39. B. Poling, J. Prausnitz, and J. O'Connell, Properties of Gases and Liquids, Fifth edition. ed. (McGraw-Hill Education, 2001), https://www.accessengineeringlibrary.com/content/book/9780070116825.

40. M. J. Pratas *et al.,* Biodiesel Density: Experimental Measurements and Prediction Models, *Energy and Fuels* **25** (2011) 2333, https://doi.org/10.1021/ef2002124.

41. L. F. Ramírez-Verduzco *et al.,* Prediction of the density and viscosity in biodiesel blends at various temperatures, *Fuel* **90** (2011) 1751, https://doi.org/10.1016/j.fuel.2010.12.032.

42. K. Krisnangkura *et al.,* An empirical approach for predicting kinematic viscosities of biodiesel blends, *Fuel* **89** (2010) 2775, https://doi.org/10.1016/j.fuel.2010.04.033.

43. J. J. Moré, The Levenberg-Marquardt algorithm: Implementation and theory (Springer, 1978), pp. 105-116, https://doi.org/10.1007/BFb0067700.

44. W. Marczak, N. Adamczyk, and M. Łężniak, Viscosity of Associated Mixtures Approximated by the Grunberg-Nissan Model, *International Journal of Thermophysics* **33** (2012) 680, https://doi.org/10.1007/s10765-011-1100-1.